

# Emergence of singularities from decoherence

Aaron Z. Goldberg,<sup>1</sup> Asma Al-Qasimi,<sup>2</sup> and D. H. J. O'Dell<sup>1</sup>

<sup>1</sup>*Department of Physics and Astronomy, McMaster University,  
1280 Main Street W., Hamilton, Ontario, Canada, L8S 4M1*

<sup>2</sup>*Department of Physics and Astronomy, University of Rochester, Rochester, New York 14627, USA.*

(Dated: December 9, 2024)

When two Bose-Einstein condensates are suddenly coupled by a tunneling junction, the Gross-Pitaevskii mean-field theory predicts that caustics will form in the number-difference probability distribution. The caustics are singular but are regularized by going to the many-body theory where atom number is quantized. However, if the system is subject to a weak continuous measurement the quantum state decoheres and classicality is restored. We investigate the emergence of singularities during the quantum-to-classical transition paying attention to the interplay between particle number  $N$  and the quantum noise introduced by the measurement.

Keywords: Catastrophe theory; Ultracold atoms, Josephson junction

Decoherence provides an explanation for why Schrödinger cat states (macroscopic quantum superpositions) are not seen in the wild: it destroys quantum interference at a rate that depends sensitively upon the ‘size’ of the superposition and thereby reduces the associated probability distribution to a sum of classical probabilities [1–3]. This occurs whenever a system becomes entangled with its environment, causing a continuously monitored quantum system to behave classically [4–7], even displaying elements of chaotic dynamics [8–11] (something which is absent in quantum mechanics). Pioneering experiments using atoms interacting with electromagnetic fields have observed the decay to classicality [12–17], including the appearance of chaos [18–21], and measurement induced suppression of tunneling [22]. Decoherence is now also actively studied in solid-state systems such as quantum dots [23], superconducting devices [24, 25], crystalline molecular magnets [26], and nitrogen-vacancy centres in diamond [27] to name just a few.

In this paper we consider the case of two atomic Bose-Einstein condensates (BECs) coupled via a tunneling barrier, i.e. a bosonic Josephson junction (BJJ), a system that has been realized in a number of experiments [28–33]. The interatomic interactions generate entanglement which manifests itself as reduced atom number fluctuations between the BECs [34–36]. This quantum resource, which can be characterized in terms of Fisher information [37], opens the door to metrology that exceeds the sensitivity of classical interferometers and has been used to perform sub-shot noise magnetometry [38]. Whilst two initially independent BECs rapidly develop a well defined relative phase as a result of an interference measurement [39–41], including the case of a weak continuous measurement via light scattering [42], when the reverse experiment is performed in which a single condensate is split in half the two pieces gradually dephase [43–45]. The effect of phase noise, which arises, e.g., from fluctuations in the relative trap depths, has been shown theoretically to decohere nonclassical states although superpositions of phase states are surprisingly stable [46].

We are interested here in the case where the number difference is measured weakly and continuously. This situation has been considered theoretically in [47] where it was shown that if the measurements are frequent enough to resolve the dynamics the measurement backaction causes the BJJ to behave classically. In the many-body context, ‘classical’ means ‘mean-field’ indicating the absence of many-body entanglement: the condensate wave function is still described by the Gross-Pitaevskii wave equation [48]. The specific dynamics we consider arise from a quench in the tunneling rate from zero to a finite value describing the conceptually important situation of when two independent condensates are suddenly placed in contact [49–51]. This sets the combined system into motion and a repeating series of collapses and partial revivals of the many-body state occur as a function of time [52, 53]. In Fock space the revivals correspond to caustics in the number-difference amplitudes which are singular in the classical limit indicating a failure of the classical theory. The singularities are removed by going to the quantum many-body theory where the discreteness of the atom number difference regularizes the caustic, an example of a quantum catastrophe [54]. However, when decoherence is included we are apparently led back to the paradoxical situation of a theory with singularities. The missing ingredient is the quantum noise introduced by the measurement backaction which we will include below using a master equation.

Catastrophe theory predicts that only certain types of singularity are structurally stable (stable against perturbations) [55–57]. These catastrophes occur generically in nature because they require no special symmetry. Examples include rainbows, the twinkling of starlight [58] and freak waves [59]. In cold atoms they have been observed in the trajectories of cold atoms in a magnetic waveguide [60], in the dynamics of a BEC in an optical lattice [61], and during reflection from an optical barrier in the presence of gravity [62]. They appear in a quenched BJJ as cusped caustics in Fock space given by the envelopes of families of classical trajectories, as shown in Fig. 1, which also illustrates their structural stability against introduc-

ing a tilt bias. Each trajectory is a solution of Josephson's equations for the number- and phase-difference [63, 64]

$$\begin{aligned}\frac{\partial z}{\partial \tau} &= -\frac{\partial H}{\partial \phi} = -\sqrt{1-z^2} \sin \phi \\ \frac{\partial \phi}{\partial \tau} &= \frac{\partial H}{\partial z} = \Lambda z + \frac{z}{\sqrt{1-z^2}} \cos \phi + \Delta E,\end{aligned}\quad (1)$$

which can be obtained as Hamilton's equations of motion from the two-mode Gross-Pitaevskii Hamiltonian

$$H = \frac{E_C}{2} \left( \frac{Nz}{2} \right)^2 - E_J \sqrt{1-z^2} \cos \phi + E_J \Delta E z. \quad (2)$$

Here,  $N$  is the total number of bosons,  $E_C$  characterizes their interactions,  $E_J$  is the coupling energy between the two BECs, and  $\Delta E$  is the tilt bias in units of the coupling energy.  $\phi = \phi_L - \phi_R$  and  $z = (N_L - N_R)/N$  are the phase- and fractional number-differences between the left- and right-hand BECs, respectively, and time is scaled as  $\tau \equiv t(2E_J/N\hbar)$ . Thus, the classical dynamics are governed by just two parameters:  $\Lambda \equiv E_C N^2 / 4E_J$  and  $\Delta E$ . In the quantum description we need to additionally specify  $N$ .

In the classical theory the conjugate variables  $z$  and  $\phi$  are continuous and commute with each other, whereas in the semiclassical theory [65] they obey the commutator  $[\hat{\phi}, \hat{z}] \approx 2i/N$ , with  $1/N$  playing the role of Planck's constant [66]. The initial state of two independent BECs corresponds to a precise value of  $z$  which we take to be zero. (By virtue of their structural stability, the caustics are qualitatively unaffected if instead we take  $z \neq 0$ . We explore this point further in the Supplementary material A.) According to Heisenberg's uncertainty relation, the initial phase must be completely undefined and so the appropriate description of the classical dynamics is an ensemble of trajectories with  $\phi$  uniformly distributed over the range  $-\pi$  to  $\pi$ . This approach corresponds to the truncated Wigner approximation where the evolution is classical but samples the initial quantum distribution [67, 68]. According to catastrophe theory, the stable singularities in the two dimensional space formed by  $z$  and  $t$  are fold lines that meet at cusp points and this is what we see in Fig. 1, where the cusp points occur periodically at the so-called plasma frequency  $\omega_{\text{pl}} = \sqrt{2E_J(2E_J + N^2 E_c/2)/N\hbar} = (2E_J/N\hbar)\sqrt{1+\Lambda}$  which gives, in the harmonic approximation, the frequency of motion around the bottom of the cosine potential well in the Hamiltonian. The density of trajectories diverges on a caustic, as shown by the thick green line in Fig. 2 which plots the probability distribution at the time  $1.5\pi/\omega_{\text{pl}}$  which occurs halfway between the first and second cusp points.

A fully quantum description of the dynamics can be achieved with the Bose-Hubbard model. A crucial difference between this and the classical treatment is that the number difference becomes quantized, recognizing the discrete nature of field quanta (atoms). No assumption of condensation is made, rather we consider two sites (L

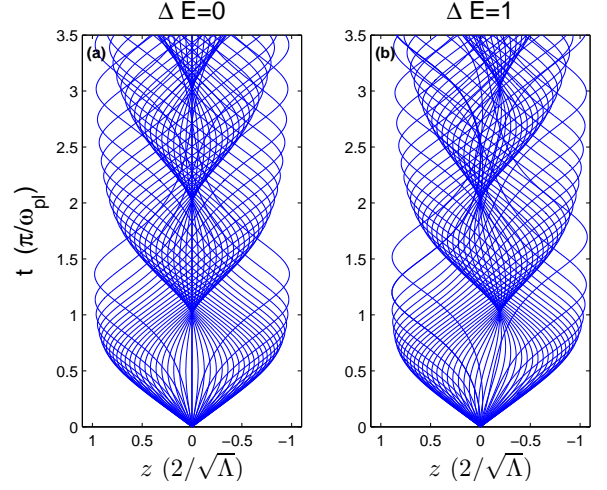


FIG. 1. Following a quench in a BJJ the classical trajectories for the fractional number difference  $z$  periodically form cusp caustics. Each trajectory has a different value of the initial phase difference ranging from  $-\pi$  to  $\pi$  in steps of  $\pi/25$  which samples the initial quantum distribution. In (a) the tilt bias  $\Delta E = 0$ , and in (b)  $\Delta E = 1$ . Having a finite tilt bias knocks the cusps off axis but due to their structural stability in two dimensions they remain as cusps.  $\Lambda = 25$  for all trajectories.

and R) occupied by bosons that are created and annihilated by the operators  $\hat{a}_L^\dagger$  ( $\hat{a}_R^\dagger$ ) and  $\hat{a}_L$  ( $\hat{a}_R$ ), obeying standard bosonic commutation relations  $[\hat{a}_i, \hat{a}_j^\dagger] = \delta_{ij}$ . In terms of these operators, the fractional number difference operator is defined as  $\hat{z} \equiv (\hat{a}_L^\dagger \hat{a}_L - \hat{a}_R^\dagger \hat{a}_R)/N$ . It is instructive to apply the Schwinger mapping [?] to angular momentum operators  $\hat{J}_x \equiv (\hat{a}_L^\dagger \hat{a}_R + \hat{a}_R^\dagger \hat{a}_L)/2$ ,  $\hat{J}_y \equiv i(\hat{a}_R^\dagger \hat{a}_L - \hat{a}_L^\dagger \hat{a}_R)/2$ , and  $\hat{J}_z \equiv (\hat{a}_L^\dagger \hat{a}_L - \hat{a}_R^\dagger \hat{a}_R)/2$  whence the Hamiltonian becomes [69]

$$\frac{\hat{H}}{2E_J/N} = \frac{N\Lambda}{4} \hat{z}^2 - \frac{1}{2} \left( \hat{a}_L^\dagger \hat{a}_R + \hat{a}_R^\dagger \hat{a}_L \right) = \frac{\Lambda}{N} \hat{J}_z^2 - \hat{J}_x \quad (3)$$

which describes a collective spin made up of the elementary spin-1/2 bosons and is a special case of the Lipkin-Meshkov-Glick model [31, 71]. In the quantum theory Fock space is discrete and finite with size  $N + 1$ . In the semiclassical theory  $N \gg 1$  so that the spectrum of  $\hat{z}$  tends towards a continuum but obeys the aforementioned canonical commutation relation with  $\hat{\phi}$  (which can be defined via the Pegg-Barnett prescription [70]) whereas in the classical limit  $N \rightarrow \infty$   $z$  is strictly continuous.

We use the Fock basis  $|z\rangle$  to represent the quantum state  $|\Psi(t)\rangle = \sum_z c_z(t) |z\rangle$  of the BJJ, evolving it from its initial state  $|z=0\rangle$  using the Schrödinger equation with the Hamiltonian given in Eq. (3). A slice through the resulting quantum probability distribution at a particular time is shown in Fig. 2, and in Fig. 4 we plot the probability distribution as a function of time in the presence of decoherence (see Fig. 1 in [54] for the decoherence-free case). The shape of the discrete probability density  $|c_z|^2$  has recognizable features in common with the classical

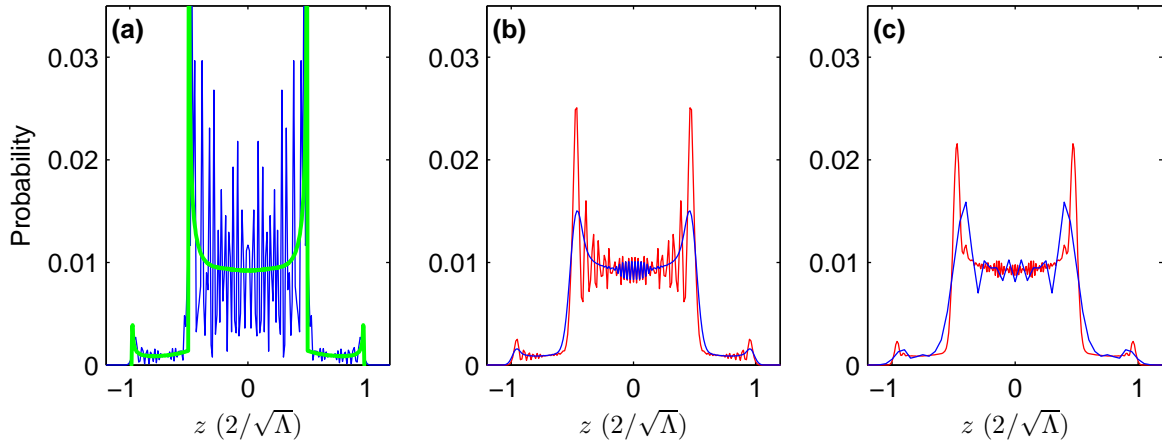


FIG. 2. Comparison of the probability distributions for the number-difference  $z$  for classical, quantum, and quantum with decoherence dynamics in a BJJ at the time slice  $t = 1.5\pi/\omega_{\text{pl}}$  with  $\Lambda = 25$ . (a) Classical (thick green line) versus the quantum with no decoherence (thin blue line), with the latter having  $N = 400$  particles. The classical probability diverges as the inverse square root of the distance from the fold caustics at  $z \approx \pm 0.5$  and  $z \approx \pm 1$ . The quantum probability distribution is actually discrete in  $z$  but drawn here with a continuous line. (b) Both distributions are for the quantum case with  $N = 400$  but with different decoherence strengths:  $D = 0.025$  (red) and  $D = 0.4$  (blue). (c) Both distributions are for the quantum case with  $D = 0.1$  but with different numbers of particles:  $N = 100$  (blue) and  $N = 500$  (red).

distribution, including peaks where it crosses the caustics (fold lines), but displays interference causing it to oscillate around the classical value. Crucially, the quantum distribution is always finite whereas the classical distribution diverges as the inverse square root of the distance from a caustic [57]. In fact, in the quantum theory the caustics are decorated by discretized Airy functions although this can be hard to see because the Airy functions from the different caustics interfere. In the semiclassical regime  $N \gg 1$ , the oscillations become very rapid and the main peaks of the Airy function come to dominate the probability distribution, growing as  $|\Psi|^2 \propto N^{1/6}$  relative to the background far from the caustic [54].

The effect of decoherence due to a weak continuous measurement of  $z$  can be incorporated into the quantum theory via the master equation [72]

$$\frac{\partial \hat{\rho}}{\partial \tau} = i \left[ \hat{J}_x, \hat{\rho} \right] - i \frac{\Lambda}{N} \left[ \hat{J}_z^2, \hat{\rho} \right] - D \frac{\Lambda}{N} \left[ \hat{J}_z, \left[ \hat{J}_z, \hat{\rho} \right] \right], \quad (4)$$

where  $D$  governs the strength of the measurement.  $\hat{\rho}(\tau)$  is the density operator which can be expanded in the Fock ( $\hat{J}_z$ ) basis as  $\hat{\rho}(t) = |\Psi(t)\rangle\langle\Psi(t)| = \sum_{q,z} \rho_{q,z}(t)|q\rangle\langle z|$ . The diagonal elements give the populations  $\rho_{z,z}(t)$  of the Fock states as plotted in Fig. 2 (b) and (c) and in Fig. 4. The master equation is in Kossakowski-Lindblad form, which ensures that the density matrix is positive-definite at all times [73, 74] (see Supplementary Material B). The double commutator is responsible for the decoherence which suppresses the density matrix's off-diagonal elements due to the gain in information about the number difference by the measurement. Experimentally, the atom number can be counted continuously (non-destructively) using phase contrast imaging [75–77].

Other techniques, such as homodyne detection when one of the two BECs is placed inside an optical cavity, have also been suggested [72].

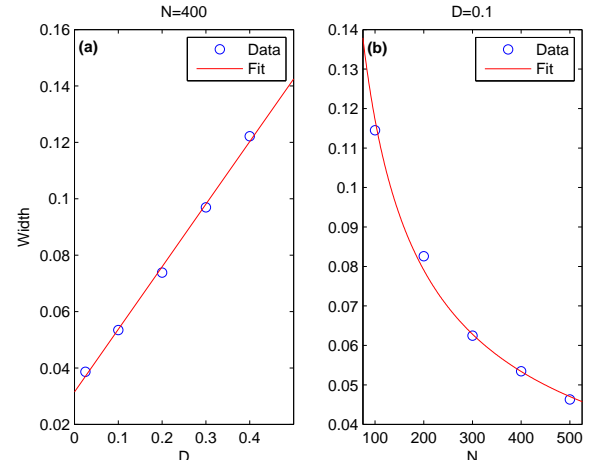


FIG. 3. Effect of varying the decoherence strength  $D$  and the number of particles  $N$  on the width of a caustic in the quantum probability distribution. The caustic in question is located at  $t = 1.5\pi/\omega_{\text{pl}}$  near  $z = -0.5$ , where  $\Lambda = 25$ . We measure the full width at three-quarters of the maximum of the peak because the half-maximum is too low for large values of  $D$  and small values of  $N$ . (a) Here  $N = 400$  and we vary  $D$ . The width of the peak increases linearly with  $D$  as  $\text{Width} = 0.2220D + 0.031503$ . (b) Here  $D = 0.1$  and we vary  $N$ . The width of the peak decreases as a power law in  $N$  as  $\text{Width} = 1.5940N^{-0.56686}$ . All of these trends are maintained if we vary the value of  $t$  but track the same fold line.

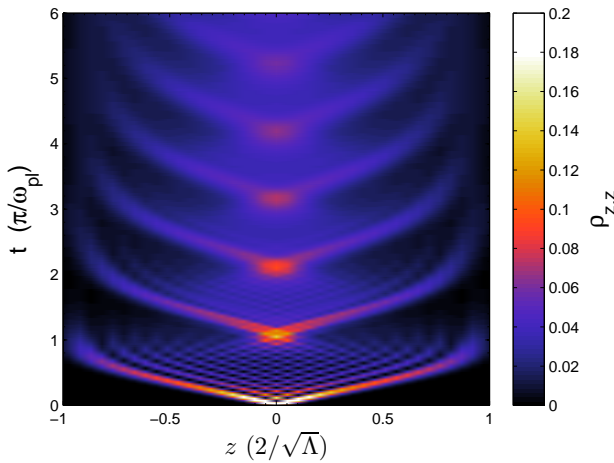


FIG. 4. Evolution of the probability distribution for the number difference ( $\rho_{z,z}$ ) over time, for  $N = 100$ ,  $\Lambda = 25$ , and  $D = 0.1$ . For this value of  $D$  the quantum interference remains visible for a few oscillations but at later times this is washed out and even the caustics are diffuse. When  $t \rightarrow \infty$  the system tends to  $\rho_{\text{steady}}$  (Eq. (5)).

Decoherence is known to smooth rapidly oscillating terms in Schrödinger dynamics [78]. In Fig. 2 we see that as  $D$  is increased the oscillations are progressively damped out and in this sense the system becomes more classical. However, we also see that the caustic peaks are softened too, signalling a departure from the classical result. By contrast, increasing  $N$  increases the sharpness of the caustics increasing the similarity with the classical distribution. These observations are quantified in Fig. 3 where the width of the caustic is found to increase linearly with  $D$  and decrease as a fractional power law with  $N$ . Furthermore, if the root mean square of the difference between the quantized probability distribution and the classical one is computed one finds that this also decreases as a power law in  $N$  (see Supplementary Material D). This suggests that the required limit for classicality is  $D \rightarrow 0$  and  $N \rightarrow \infty$  but such that  $D \times N$  is always finite. Another interesting limit is the long-time limit for fixed  $D$  and  $N$ . In this case the density matrix becomes diagonal and the probability distribution tends to a steady state which is flat (see Supplementary Material C)

$$\langle q | \rho_{\text{steady}} | z \rangle \equiv \rho_{\text{steady},q,z} = \frac{\delta_{q,z}}{N+1}. \quad (5)$$

This behavior can be seen in Fig. 4 where we see the caustics gradually dissipate.

The authors of Reference [47] also consider a BJJ but with a slightly different measurement scheme and dynam-

ics. They shed light on the effect of decoherence by deriving an equation of motion for the Wigner quasiprobability distribution and showing that the decoherence produces terms that give rise to diffusion with  $D$  playing the role of a diffusion constant. The origin of the diffusion is quantum noise introduced by the measurement backaction. Considering instead the time evolution of the Glauber-Surdashan  $P$  distribution in phase space, which has the slight advantage of always being positive if the quantum system has a classical analogue, we obtain the equation (see Supplementary Material E)

$$\frac{\partial P}{\partial \tau} = 4 \left[ - \left( \frac{\partial H}{\partial \phi} \right) \partial_z + \left( \frac{\partial H}{\partial z} \right) \partial_\phi + 2 \frac{D\Lambda}{N} \partial_\phi^2 \right] P \quad (6)$$

where the Hamiltonian is scaled such that  $H = \Lambda z^2/2 - \sqrt{1-z^2} \cos \phi$ . The diffusion term in this equation is responsible for two effects: it eliminates quantum interference such that the probability distribution settles to the classical distribution, and it broadens the peaks at the caustics such that the resultant probability distributions remain non-singular at all times, thus resolving the paradox that decoherence can lead to singularities.

*Conclusions* Classical theories breakdown at caustics where they predict singularities. Furthermore, catastrophe theory predicts that caustics are generic due to their structural stability. In the many-body case the singularity is in the probability distribution in Fock space rather than the more tangible coordinate space, but nevertheless this represents a striking failure. If decoherence merely reduced the quantum prediction to the classical one this would spell trouble because true singularities would exist even in finite systems ( $N \neq \infty$ ). Caustics therefore represent a particularly stern test of decoherence theory. However, decoherence is more subtle and softens the singularity by means of diffusion due to quantum noise. At any finite  $N$  the results of decoherence will therefore be finite. In the thermodynamic limit ( $N \rightarrow \infty$ ) singularities are allowed, although without decoherence the quantum probability distribution will oscillate infinitely fast. In the ‘old’ way of taking the classical limit the oscillations were presumed averaged out by the finite resolution of a detector [79], but with decoherence the true classical limit (which must include caustics) is obtained by letting  $N \rightarrow \infty$  while keeping  $D > 0$  so that oscillations are washed out but the singularities are maintained.

## ACKNOWLEDGMENTS

We acknowledge funding from the Natural Sciences and Engineering Research Council of Canada.

[1] W. H. Zurek, Phys. Today **44**, 36 (1991).

[2] W. H. Zurek, Rev. Mod. Phys. **75**, 715 (2003).

[3] M. Schlosshauer, Rev. Mod. Phys. **76**, 1267 (2005).

[4] E. Joos and H. D. Zeh, Z. Phys. B **59** 223 (1985).

[5] W. H. Zurek and J. P. Paz, Phys. Rev. Lett. **72**, 2508 (1994).

[6] W. H. Zurek, S. Habib, and J. P. Paz, Phys. Rev. Lett. **70**, 1187 (1993).

[7] M. R. Gallis, Phys. Rev. A **53**, 655 (1996).

[8] T. P. Spiller and J. F. Ralph, Phys. Lett. A **194** A235 (1994).

[9] S. Habib, K. Shizume, and W. H. Zurek, Phys. Rev. Lett. **80**, 4361 (1998).

[10] T. Bhattacharya, S. Habib, and K. Jacobs, Phys. Rev. Lett. **85**, 4852 (2000).

[11] Z. P. Karkuszewski, C. Jarzynski, and W. H. Zurek, Phys. Rev. Lett. **89**, 170405 (2002).

[12] M. Brune, E. Hagley, J. Dreyer, X. Maitre, C. Wunderlich, J. M. Raimond, and S. Haroche, Phys. Rev. Lett. **77**, 4887 (1996).

[13] C. J. Myatt, B. E. King, Q. A. Turchette, C. A. Sackett, D. Kielpinski, W. M. Itano, C. Monroe, and D. J. Wineland, Nature (London) **403**, 269 (2000).

[14] Q. A. Turchette, C. J. Myatt, B. E. King, C. A. Sackett, D. Kielpinski, W. M. Itano, C. Monroe, and D. J. Wineland, Phys. Rev. A **62**, 053807 (2000).

[15] D. A. Kokorowski, A. D. Cronin, T. D. Roberts, and D. E. Pritchard, Phys. Rev. Lett. **86**, 2191 (2001).

[16] K. Hornberger, S. Uttenthaler, B. Brezger, L. Hackermüller, M. Arndt, and A. Zeilinger, Phys. Rev. Lett. **90**, 160401 (2003).

[17] S. Deléglise, I. Dotsenko, C. Sayrin, J. Bernu, M. Brune, J-M. Raimond and S. Haroche, Nature (London), **455**, 510 (2008).

[18] D. A. Steck, W. H. Oskay, and M. G. Raizen, Science **293**, 274 (2001).

[19] W. K. Hensinger, H. Häffner, A. Browaeys, N. R. Heckenberg, K. Helmerson, C. McKenzie, G. J. Milburn, W. D. Phillips, S. L. Rolston, H. Rubinsztein-Dunlop, and B. Upcroft, Nature (London) **412**, 52 (2001).

[20] D. A. Steck, W. H. Oskay, and M. G. Raizen, Phys. Rev. Lett. **88**, 120406 (2002).

[21] S. Chaudhury, A. Smith, B. E. Anderson, S. Ghose, and P. S. Jessen, Nature (London), **461**, 768 (2009).

[22] Y. S. Patil, S. Chakram, and M. Vengalattore, Phys. Rev. Lett. **115**, 140402 (2015).

[23] P. Borri, W. Langbein, S. Schneider, U. Woggon, R. L. Sellin, D. Ouyang, and D. Bimberg, Phys. Rev. Lett. **87**, 157401 (2001).

[24] G. Ithier, E. Collin, P. Joyez, P. J. Meeson, D. Vion, D. Esteve, F. Chiarello, A. Shnirman, Y. Makhlin, J. Schriefl, and G. Schön, Phys. Rev. B **72**, 134519 (2005).

[25] J. Claudon, A. Fay, L. P. Lévy, and O. Buisson, Phys. Rev. B **73**, 180502(R) (2006).

[26] S. Takahashi, I. S. Tupitsyn, J. van Tol, C. C. Beedle, D. N. Hendrickson, and P. C. E. Stamp, Nature (London) **476**, 76 (2011).

[27] S. Putz, D. O. Krimer, R. Amsüss1, A. Valookaran, T. Nöbauer, J. Schmiedmayer, S. Rotter, and J. Majer, Nature Phys. **10** (2014).

[28] M. Albiez, R. Gati, J. Fölling, S. Hunsmann, M. Cristiani, and M. K. Oberthaler, Phys. Rev. Lett. **95**, 010402 (2005).

[29] T. Schumm, S. Hofferberth, L. M. Andersson, S. Wildermuth, S. Groth, I. Bar-Joseph, J. Schmiedmayer, and P. Krüger, Nature Phys. **1**, 57 (2005).

[30] S. Levy, E. Lahoud, I. Shomroni, and J. Steinhauer, Nature **449**, 579 (2007).

[31] T. Zibold, E. Nicklas, C. Gross, and M. K. Oberthaler, Phys. Rev. Lett. **105**, 204101 (2010).

[32] L. J. LeBlanc, A. Bardon, J. McKeever, M. Extavour, D. Jervis, J. Thywissen, F. Piazza, and A. Smerzi, Phys. Rev. Lett. **106**, 025302 (2011).

[33] A. Trenkwalder, G. Spagnoli, G. Semeghini, S. Coop, M. Landini, P. Castilho, L. Pezzè, G. Modugno, M. Inguscio, A. Smerzi and M. Fattori, Nat. Phys. (2016), arXiv:1603.02979

[34] C. Orzel, A. K. Tuchman, M. L. Fenselau, M. Yasuda, M. A. Kasevich, Science **291**, 2386 (2001).

[35] J. Estève, C. Gross, A. Weller, S. Giovanazzi, and M. K. Oberthaler, Nature (London) **455**, 1216 (2008).

[36] C. Gross, T. Zibold, E. Nicklas, J. Estève, and M. K. Oberthaler, Nature (London) **464**, 1165 (2010).

[37] H. Strobel, W. Muessel, D. Linnemann, T. Zibold, D. B. Hume, Luca Pezzè, A. Smerzi, and M. K. Oberthaler, Science **345**, 424 (2014).

[38] W. Muessel, H. Strobel, D. Linnemann, D. B. Hume, and M. K. Oberthaler, Phys. Rev. Lett. **113**, 103004 (2014).

[39] J. I. Cirac, C. W. Gardiner, M. Naraschewski, and P. Zoller, Phys. Rev. A **54** R3714 (1996).

[40] M. R. Andrews, C. G. Townsend, H.-J. Miesner, D. S. Durfee, D. M. Kurn, W. Ketterle, Science ?? **275**, 637 (1997).

[41] Y. Castin and J. Dalibard, Phys. Rev. A **55** 4330 (1997).

[42] M. Saba, T. A. Pasquini, C. Sanner, Y. Shin, W. Ketterle, and D. E. Pritchard, Science **307**, 1945 (2005).

[43] M. Gring, M. Kuhnert, T. Langen, T. Kitagawa, B. Rauer, M. Schreitl, I. Mazets, D. Adu Smith, E. Demler, and J. Schmiedmayer, Science **337**, 1318 (2012).

[44] D. Adu Smith, M. Gring, T Langen, M. Kuhnert, B. Rauer, R. Geiger, T. Kitagawa, I. Mazets, E. Demler and J. Schmiedmayer, New J. Phys. **15**, 075011 (2013).

[45] T. Langen, R. Geiger, M. Kuhnert, B. Rauer, and J. Schmiedmayer, Nature Phys. **9**, 640 (2013).

[46] G. Ferrini, D. Spehner, A. Minguzzi, and F. W. J. Hekking, Phys. Rev. A **82**, 033621 (2010).

[47] J. Javanainen and J. Ruostekoski, New J. Phys. **15**, 013005 (2013).

[48] L. Pitaevskii and S. Stringari, Phys. Rev. Lett. **87**, 180402 (2001).

[49] I. Zapata, F. Sols, and A. J. Leggett, Phys. Rev. A **67**, 021603(R) (2003).

[50] H. Xiong, S. Liu, and M. Zhan, Phys. Rev. B **73**, 224505 (2006).

[51] M. Trujillo-Martinez, A. Posazhennikova, and J. Kroha, Phys. Rev. Lett. **103**, 105302 (2009).

[52] G. J. Milburn, J. Corney, E. M. Wright, D. F. Walls, Phys. Rev. A **55**, 4318 (1997).

[53] H. Veksler and S. Fishman, New J. Phys. **17**, 053030 (2015).

[54] D. H. J. O'Dell, Phys. Rev. Lett. **109** (2012).

[55] R. Thom, *Structural Stability and Morphogenesis* (Benjamin, Reading, MA, 1975).

[56] V.I. Arnold, Russ. Math. Survs. **30**, 1 (1975).

[57] M. Berry, *Singularities in Waves and Rays* in Les Houches, Session XXXV, 1980 *Physics of Defects*, edited by R. Balian et al. (North Holland Publishing, Amsterdam, 1981).

[58] M. V. Berry, J. Phys. A: Math. Gen. **10**, 2061 (1977).

[59] R. Höhmann, U. Kuhl, H.-J. Stöckmann, L. Kaplan, and E. J. Heller, Phys. Rev. Lett. **104**, 093901 (2010).

[60] W. Rooijakkers, S. Wu, P. Striehl, M. Vengalattore, and

M. Prentiss, Phys. Rev. A **68**, 063412 (2003).

[61] J. H. Huckans, I. B. Spielman, B. L. Tolra, W. D. Phillips, and J. V. Porto, Phys. Rev. A **80**, 043609 (2009).

[62] S. Rosenblum, O. Bechler, I. Shomroni, R. Kaner, T. Arusi-Parpar, O. Raz, and B. Dayan, Phys. Rev. Lett. **112**, 120403 (2014).

[63] A. Smerzi, S. Fantoni, S. Giovanazzi, and S. R. Shenoy, Phys. Rev. Lett. **79**, 4950 (1997).

[64] S. Raghavan, A. Smerzi, S. Fantoni, and S. Shenoy, Phys. Rev. A **59**, 620 (1999).

[65] G. J. Krahn and D. H. J. ODell, J. Phys. B: At. Mol. Opt. Phys. **42**, 205501 (2009).

[66] A. Vardi and J. R. Anglin, Phys. Rev. Lett. **86**, 568 (2001).

[67] A. Sinatra, C. Lobo, and Y. Castin, J. Phys. B **35**, 3599 (2002).

[68] A. Polkovnikov, Phys. Rev. A **68**, 053604 (2003).

[69] A. P. Hines, R. H. McKenzie, and G. J. Milburn, Phys. Rev. A **67**, 013609 (2003).

[70] G.-S. Paraoanu, S. Kohler, F. Sols and A. J. Leggett, J. Phys. B: At. Mol. Opt. Phys. **34**, 4689 (2001).

[71] H.J. Lipkin, N. Meshkov, and A. J. Glick, Nucl. Phys. **62**, 188 (1965).

[72] J. F. Corney and G. J. Milburn, Phys. Rev. A **58**, 2399 (1998).

[73] G. Lindblad, Comm. Math. Phys. **48**, 119 (1976).

[74] V. Gorini, A. Frigerio, M. Verri, A. Kossakowski, and E. Sudarshan, Rep. Math. Phys. **13**, 149 (1978).

[75] C. C. Bradley, C. A. Sackett, and R. G. Hulet, Phys. Rev. Lett. **78**, 985 (1997).

[76] M. R. Andrews, M.-O. Mewes, N. van Druten, D. Durfee, D. Kurn, and W. Ketterle, Science **273**, 84 (1996).

[77] M. R. Andrews, D. M. Kurn, H.-J. Miesner, D. S. Durfee, C. G. Townsend, S. Inouye, and W. Ketterle, Phys. Rev. Lett. **79**, 553 (1997).

[78] R. Kosloff, Entropy **15**, 2100 (2013).

[79] M. V. Berry and K. E. Mount, Reps. Prog. Phys. **35**, 315 (1972).

## Supplementary Material

### Appendix A: Stability to changes in initial conditions

With the second-quantized formulation we initialize a Gaussian superposition of states

$$c_z = \frac{1}{Z} e^{-\frac{z^2 N^2}{8\sigma^2}}, \quad (\text{A1})$$

where

$$Z = \sqrt{\sum_z c_z^2}. \quad (\text{A2})$$

These initial conditions are then evolved using the Schrödinger equation with the Hamiltonian Eq. (3). For values of  $\sigma$  up to 1/2, the behaviour is nearly identical to starting in the  $z = 0$  state (Fig. 5a). Since these initial conditions are highly similar to  $|0\rangle$ , this verifies the stability prediction of catastrophe theory.

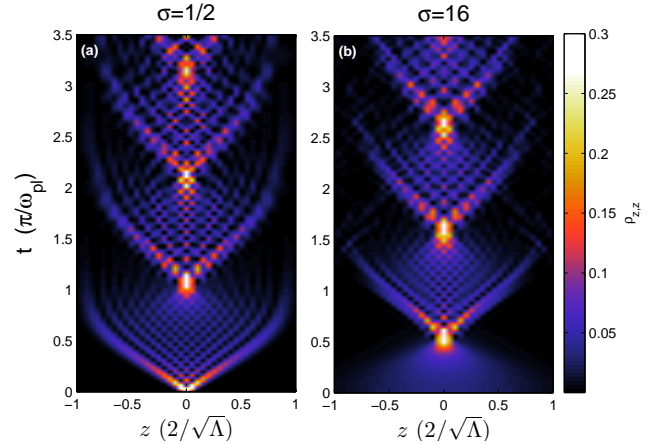


FIG. 5. Stability of the catastrophe structures to varying the width of the initial state in Fock space. Evolution of the 100-particle system with  $\Lambda = 25$ , in the initial state given by Eq. (A1). **a.** With the initial width  $\sigma = 1/2$ , the behaviour is quite similar to the  $z = 0$  initial condition case. **b.** Increasing the initial width to  $\sigma = 16$  again yields the catastrophe structures, which now begin at  $t = 0.5\pi/\omega_{\text{pl}}$ .

Large  $\sigma$  values correspond to starting in a state with maximal uncertainty in  $z$  but minimal uncertainty in  $\phi$ , and the initial cusp moves to a later time  $t > 0$ . (Fig. 5b). These show the robustness of the result that the second-quantized dynamics oscillate around the mean-field dynamics while remaining finite at the caustics.

We note that the pixelation in Fig. 5 is not a resolution limit, but rather the result of  $z$  being quantized. It is this very quantization that corrects the classical results through a quantized Airy function.

### Appendix B: Form of the master equation

We here show that Eq. (4) is in Kossakowski-Lindblad form. This is the most general form that ensures the positivity of the reduced density matrix  $\rho_S$  at all times, where

$$\rho_S = \text{Tr}_E [\rho_{SE} (t)], \quad (\text{B1})$$

and  $S$ ,  $E$ , and  $SE$  denote the system, environment, and composite system, respectively [3]. We rewrite the master equation in this general form by defining the Lindblad superoperator  $\mathcal{L}$

$$\mathcal{L}\rho = L\rho L^\dagger - \frac{1}{2} (\rho L^\dagger L + L^\dagger L\rho). \quad (\text{B2})$$

With

$$L = L^\dagger \equiv \sqrt{2D\Lambda/N} J_z \quad (\text{B3})$$

and the reduced Hamiltonian

$$\tilde{H} \equiv -J_x + \frac{\Lambda}{N} J_z^2, \quad (\text{B4})$$

we see that the promised equation

$$\dot{\rho} = -i [\tilde{H}, \rho] - \mathcal{L}\rho. \quad (\text{B5})$$

is equivalent to our master equation

$$\frac{\partial \rho}{\partial \tau} = i [J_x, \rho] - i \frac{\Lambda}{N} [J_z^2, \rho] - D \frac{\Lambda}{N} [J_z, [J_z, \rho]]. \quad (\text{B6})$$

### Appendix C: Steady state derivation

The master equation can be expressed in the number difference basis as

$$\begin{aligned} \frac{d \rho_{q,z}}{d \tau} = & i \frac{N \Lambda}{4} \rho_{q,z} (z^2 - q^2) \\ & - i \frac{N}{4} \left[ \rho_{q,z+1} \sqrt{\left(1 + z + \frac{2}{N}\right)(1 - z)} \right. \\ & + \rho_{q,z-1} \sqrt{\left(1 - z + \frac{2}{N}\right)(1 + z)} \\ & - \rho_{q+1,z} \sqrt{\left(1 + q + \frac{2}{N}\right)(1 - q)} \\ & \left. - \rho_{q-1,z} \sqrt{\left(1 - q + \frac{2}{N}\right)(1 + q)} \right] \\ & - D \frac{N \Lambda}{4} \rho_{q,z} (q - z)^2. \end{aligned} \quad (\text{C1})$$

Choosing, e.g.,  $z = q - 1$  yields

$$\begin{aligned} \dot{\rho}_{q,q-1} = & i \frac{N \Lambda}{4} \rho_{q,q-1} (-2q + 1) \\ & - i \frac{N}{4} \left[ \rho_{q,q} \sqrt{(1 + q)(1 - q + \frac{2}{N})} \right. \\ & + \rho_{q,q-2} \sqrt{\left(1 - q + \frac{4}{N}\right)\left(1 + q - \frac{2}{N}\right)} \\ & - \rho_{q+1,q-1} \sqrt{\left(1 + q + \frac{2}{N}\right)(1 - q)} \\ & \left. - \rho_{q-1,q-1} \sqrt{\left(1 - q + \frac{2}{N}\right)(1 + q)} \right] \\ & - D \frac{N \Lambda}{4} \rho_{q,q-1}. \end{aligned} \quad (\text{C2})$$

By inspection of (C1) with this case, the off-diagonal terms should decay to zero exponentially with increasing  $\tau$ . Setting the time derivative to 0 and retaining only the diagonal elements of  $\rho$  yields

$$\rho_{q,q} = \rho_{q-1,q-1}, \quad (\text{C3})$$

and so

$$\rho_{\text{steady } q,z} = \frac{\delta_{q,z}}{N + 1}, \quad (\text{C4})$$

where we have employed the normalization condition  $\text{Tr}[\rho] = 1$ .

Alternatively, one can observe that  $\langle q | [J_z, [J_z, \rho]] | z \rangle = (J_{z,q,q} - J_{z,z,z})^2 \rho_{q,z}$  is only identically zero when  $\rho_{q,z} = 0$  for all  $q \neq z$ , ensuring that the steady state is diagonal in the Fock basis. Elementary commutator algebra shows that

$$\begin{aligned} \langle q | [H, \rho] | z \rangle &= \sum_j H_{q,j} \rho_{j,z} - \rho_{q,j} H_{j,z} \\ &= H_{q,z} (\rho_{z,z} - \rho_{q,q}) \end{aligned} \quad (\text{C5})$$

for  $\rho$  being diagonal. This commutator is only identically zero when  $\rho_{q,q} = \rho_{z,z}$ , which is the steady state derived above.

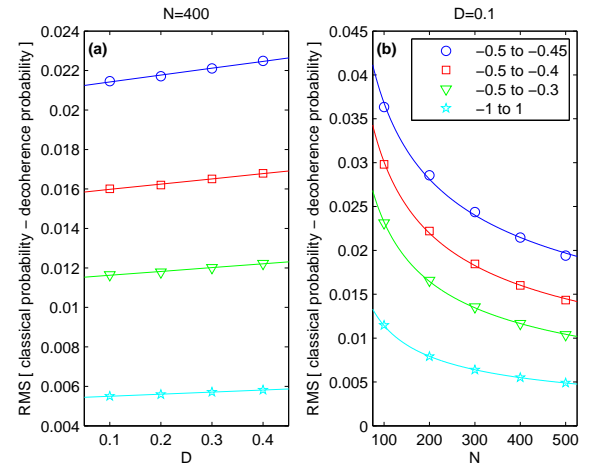


FIG. 6. Comparison of the classical probability distribution to the quantum distribution for varying decoherence strength and number of particles. Root-mean-square (RMS) of the difference between the classical probability distribution (Fig. 2a) versus **a.**  $D$  and **b.**  $N$ , for  $\Lambda = 25$  and time  $t\omega_{\text{pl}} = 1.5\pi$ . The RMS is calculated for various ranges of  $z$ , all of which show the same trends. Since the inside of a caustic is well-studied by catastrophe theory [?], we use ranges between the caustic at  $z = -0.5$  and the three locations  $z = -0.45$  (blue circles),  $z = -0.4$  (red squares), and  $z = -0.3$  (green triangles), as well as the range  $-1 \leq z \leq 1$  (cyan stars). **a.** Here  $N = 400$ . For all ranges of  $z$ , the difference between the classical probability and the probability with decoherence increases linearly with  $D$ . The fits are as follows:  $-0.5 \text{ to } -0.45$  has RMS =  $0.0034789D + 0.021073$ ;  $-0.5 \text{ to } -0.4$  has RMS =  $0.0026552D + 0.015714$ ;  $-0.5 \text{ to } -0.3$  has RMS =  $0.0019387D + 0.011435$ ; and,  $-1 \text{ to } 1$  has RMS =  $0.0010545D + 0.0053897$ . **b.** Here  $D = 0.1$ . For all ranges of  $z$ , the difference between the classical probability and the probability with decoherence decreases as a power-law in  $N$ . The fits are as follows:  $-0.5 \text{ to } -0.45$  has RMS =  $0.2204N^{-0.38864}$ ;  $-0.5 \text{ to } -0.4$  has RMS =  $0.2436N^{-0.45413}$ ;  $-0.5 \text{ to } -0.3$  has RMS =  $0.2298N^{-0.49752}$ ; and,  $-1 \text{ to } 1$  has RMS =  $0.1302N^{-0.5283}$ . All of the above trends are conserved while varying the value of  $t$ .

## Appendix D: Quantifying the return to classicality

Here we investigate further the effects of varying decoherence strength  $D$  and particle number  $N$  on obtaining the classical limit from the system with decoherence. We use the root-mean-squared (RMS) difference between the classical and quantum probability distributions to measure the return to classicality, ensuring that our measurement is not obscured by an averaging effect. Fig. 6 plots this measurement versus  $D$  and  $N$  for various ranges in  $z$ . Three of the ranges focus on the inside edge of the caustic, and the fourth looks at the entire range  $-1 \leq z \leq 1$ . We find that the RMS value increases linearly with  $D$  and decreases as a power-law in  $N$ , the same trend as the widths of the peaks in Fig. 3. The trend is seen not only on the inside edge of the caustic, but also across the entire range  $-1 \leq z \leq 1$ . We see again that increasing decoherence slowly pushes the system away from the classical distribution, and that increasing the number of particles while decoherence is turned on rapidly pushes the system toward classicality.

## Appendix E: Derivation of the Fokker-Planck equation

Here we derive a Fokker-Planck equation from the master equation Eq. (4) using the P-representation (following Breuer & Petruccione or Gardiner & Zoller 2004). The authors of Ref. [47] did a calculation for a similar system using the related Wigner function method, for a different measurement scheme. We define the probability density function  $P(\alpha, \alpha^*, \beta, \beta^*; t)$  by

$$\rho(t) = \int d^2\alpha d^2\beta P(\alpha, \alpha^*, \beta, \beta^*; t) |\alpha\rangle\langle\alpha| |\beta\rangle\langle\beta| \quad (\text{E1})$$

for coherent states

$$|\alpha\rangle = \exp(\alpha a_L^\dagger - \alpha^* a_L) |0\rangle \quad (\text{E2})$$

and

$$|\beta\rangle = \exp(\beta a_R^\dagger - \beta^* a_R) |0\rangle. \quad (\text{E3})$$

This can be substituted into Eq. (4) using the correspondences

$$\begin{aligned} a_L \rho &\leftrightarrow \alpha P, a_L^\dagger \rho \leftrightarrow (\alpha^* - \partial_\alpha) P, \rho a_L \leftrightarrow (\alpha - \partial_{\alpha^*}) P, \rho a_L^\dagger \leftrightarrow \alpha^* P \\ a_R \rho &\leftrightarrow \beta P, a_R^\dagger \rho \leftrightarrow (\beta^* - \partial_\beta) P, \rho a_R \leftrightarrow (\beta - \partial_{\beta^*}) P, \rho a_R^\dagger \leftrightarrow \beta^* P \end{aligned} \quad (\text{E4})$$

to yield

$$\begin{aligned} \frac{dP}{d\tau} = & \left( \frac{i}{2} (\alpha^* \partial_{\beta^*} - \alpha \partial_\beta + \beta^* \partial_{\alpha^*} - \beta \partial_\alpha) \right. \\ & - i \frac{\Lambda}{4N} [-2(\alpha\alpha^* - \beta\beta^*) (\alpha\partial_\alpha - \alpha^*\partial_{\alpha^*} + \beta^*\partial_{\beta^*} - \beta\partial_\beta) + \alpha\partial_\alpha - \right. \\ & \left. \alpha^2 \partial_\alpha^2 - \alpha^{*2} \partial_{\alpha^*}^2 + \beta^2 \partial_\beta^2 - \beta^{*2} \partial_{\beta^*}^2 + \alpha\partial_\alpha\beta\partial_\beta - \alpha^*\partial_{\alpha^*}\beta^*\partial_{\beta^*}] \right. \\ & \left. + \frac{D\Lambda}{4N} \left\{ -\frac{1}{2} [(\alpha^* \partial_{\alpha^*} - \alpha \partial_\alpha)^2 + (\beta^* \partial_{\beta^*} - \beta \partial_\beta)^2] + (\alpha^* \partial_{\alpha^*} - \alpha \partial_\alpha)^2 \right\} \right) P \end{aligned} \quad (\text{E5})$$

Next we transform to the real variables  $z$  and  $\phi$

$$\alpha \equiv \sqrt{\frac{N}{2}(1-z)} \exp\left(-\frac{i\phi}{2}\right), \beta \equiv \sqrt{\frac{N}{2}(1+z)} \exp\left(\frac{i\phi}{2}\right), \quad (\text{E6})$$

as per Reference [47]. We compute

$$\partial_\alpha = \frac{2}{\alpha} [(z-1) \partial_z + i \partial_\phi] \quad (\text{E7})$$

and

$$\partial_\beta = \frac{2}{\beta} [(z+1) \partial_z - i \partial_\phi], \quad (\text{E8})$$

noting that  $(\partial_\alpha)^* = \partial_{\alpha^*}$ , etc. We substitute into Eq. (E5) to yield

$$\begin{aligned} \frac{\partial P}{\partial \tau} = & \left[ -4\sqrt{1-z^2} \sin \phi \partial_z + 4 \frac{z}{\sqrt{1-z^2}} \cos \phi \partial_\phi + 4\Lambda z \partial_\phi + 8 \frac{D\Lambda}{N} \partial_\phi^2 \right] P \\ = & 4 \left[ -\left( \frac{\partial H}{\partial \phi} \right) \partial_z + \left( \frac{\partial H}{\partial z} \right) \partial_\phi + 2 \frac{D\Lambda}{N} \partial_\phi^2 \right] P \end{aligned} \quad (\text{E9})$$

for

$$H = \frac{\Lambda z^2}{2} - \sqrt{1-z^2} \cos \phi. \quad (\text{E10})$$